Wood Science and Technology
https://doi.org/10.1007/s00226-020-01178-1

ORIGINAL

Comparison of two forensic wood identification technologies for ten Meliaceae woods: computer vision versus mass spectrometry

Prabu Ravindran[1] · **Alex C. Wiedenhoeft**[1,2,3,4]

Received: 31 December 2019

Abstract

A wealth of forensic wood identification technologies has been developed or improved in recent years, with many attempts to compare results between technologies. The utility of such comparisons is greatly reduced when the species tested with each technology are different and when performance metrics are not calculated or presented in the same way. Here, a species-level XyloTron computer vision model is presented along with a side-by-side comparison for species- and genus-level identification of the 10 species of Meliaceae studied by Deklerck et al. using mass spectrometry. The species-level accuracies of the XyloTron model and the mass spectrometry models are comparable, while the genus-level accuracy of the XyloTron model is higher than that of the mass spectrometry model. The paper concludes with a call for better practices to compare disparate forensic wood identification technologies from a performance driven perspective.

✉ Prabu Ravindran
pravindran@wisc.edu

Alex C. Wiedenhoeft
awiedenhoeft@fs.fed.us

[1] Department of Botany, University of Wisconsin, Madison, WI 53706, USA

[2] Forest Products Laboratory, Center for Wood Anatomy Research, USDA Forest Service, Madison, WI 53726, USA

[3] Department of Forestry and Natural Resources, Purdue University, West Lafayette, IN 47907, USA

[4] Ciências Biológicas (Botânica), Universidade Estadual Paulista–Botucatu, São Paulo, Brazil

Published online: 04 July 2020

Introduction

A wide range of contexts drives the need for scientifically rigorous forensic wood identification technologies, including the identification of cultural property (Ruffinatto et al. 2010; Ostapkowicz et al. 2017; Guo et al. 2019), determination of structure–property wood technology relationships (Wiedenhoeft and Kretschmann 2014), analysis of evidence from criminal forensic contexts (Graham 1997), and investigation of forest products supply chains (Wiedenhoeft et al. 2019). With the sustained interest in enforcing national and international laws and treaties to control trade in endangered species and ensure legal timber trade, evaluating the validity, reliability, and contextual applicability of various wood forensic techniques is more important than ever.

The primary scientific questions for any forensic wood identification technology are geographic origin and botanical identification. The former question has been primarily addressed by stable isotope methods (Kagawa and Leavitt (2010) and reviewed in Meier-Augenstein (2019)], DNA-based methods (e.g., Degen et al. 2013; Vlam et al. 2018), and chemometric methods (Bergo et al. 2016; Finch et al. 2017; Ma et al. 2018), with recent work showing newfound applicability of wood anatomy for this question (Akhmetzyanov et al. 2019). The latter questions historically have been addressed by traditional anatomical wood identification, either field-level identification with a hand lens, a typically coarse resolution and exclusionary identification in the context of a specific product claim (e.g., the unknown wood is not consistent with the product claim), or with finer-scale resolution and typically positive identification in the laboratory with a light microscope, generally to a generic or subgeneric level of specificity (Gasson 2011). Approaches other than traditional wood anatomy include computer vision (Khalid et al. 2008; Filho et al. 2014; Rosa da Silva et al. 2017; Ravindran et al. 2018), molecular methods such as DNA barcoding (Jiao et al. 2018), and wood extractive-based methods including spectroscopic methods like NIRS (Snel et al. 2018; Ma et al. 2018) or LIBS (Cordeiro et al. 2012), mass spectrometry methods such as direct analysis in real time (DART) (reviewed in Pavlovich et al. 2018), GC–MS (Kite et al. 2010; Zhang et al. 2019), and additional technologies including electronic (Cordeiro et al. 2012) and biological (Braun 2013) noses.

There have been calls for integration and application of methods and technologies to combat illegal logging for a number of years (Dormontt et al. 2015; Lowe et al. 2016), but one of the factors limiting the ability to appropriately combine technologies or select which approaches are best suited for any specific application is the general lack of intercomparability of data sets. With disparate reference taxa tested across different technologies, direct and objective comparison of the relative strengths of different approaches is not possible.

Not all reference taxa are equal—it is routine to separate *Quercus rubra* from *Quercus alba*, but separating *Swietenia macrophylla* from *Swietenia mahagoni* was until recently (He et al. 2019) considered impossible by wood anatomy. Likewise with DNA barcoding, plants often fail to be separated at the species level using "standard" plant DNA barcodes (Kress 2017), necessitating the

development of additional barcodes (Jiao et al. 2019). It should similarly be expected that biological variability and broad biological characteristics of different woods will inform the resolving power of other forensic technologies, including determination of geographic origin by stable isotope analysis, and botanical identification by extractive chemistry. No technique, regardless of its technical resolution, can validly discover or capitalize on biological variability that does not exist in the reference data set. A necessary first step in comparing forensic wood identification technologies is to evaluate them on the same species using the same metrics, with identification accuracy being the one easily comparable across technologies.

In order to provide an example of *Malus*-to-*Malus* evaluation of two wood identification technologies, a species-level XyloTron computer vision wood identification model was developed for the same set of ten species studied in a recent DART mass spectrometry paper (Deklerck et al. 2019). Results of the XyloTron model, based on specimens from xylaria, are presented side-by-side with those of Deklerck et al. (2019) evaluated at the species and the genus level. Comparison in this way allows objective evaluation of the accuracy of each technology at the two different taxonomic scales, which can inform practical, context-dependent deployment strategies.

Materials and methods

Dataset

The transverse surfaces of 193 wood specimens for 10 species (the same species as in Deklerck et al. 2019) from the family Meliaceae were prepared for macroscopic imaging. Using a customized implementation of the open-source XyloTron system, at least 5 non-overlapping 2048×2048 pixel, 8-bit RGB images, per specimen, of the prepared transverse surfaces were obtained using a XyloScope (Hermanson et al. 2019). Each image represents 6.35 mm $\times$ 6.35 mm of tissue, and imaging parameters were identical to those in Ravindran et al. (2018). The wood specimens used in the dataset are listed in Table 1.

Model architecture

The convolutional neural network (CNN, LeCun et al. 1989) used here consisted of an ImageNet (Russakovsky et al. 2015) pretrained ResNet34 (He et al. 2016) backbone that included all the residual blocks with a customized head. The customized head included global average and max pooling layers, whose outputs were concatenated and passed through two modules each consisting of batchnorm (Ioffe and Szegedy 2015), dropout (Hinton et al. 2012), and fully connected/linear layers (BDL) in sequence (Fig. 1). ReLU (Nair and Hinton 2010) and softmax activations were used after the linear layers in the two BDL modules (represented as L_r and L_s, respectively, in Fig. 1). This CNN architecture was also used in Ravindran et al. (2019) and was not optimized for this data set.

Table 1 The 10 Meliaceae species and the xylarium specimens included in the data set. Specimens are listed based on their fold membership

Species	Accession identifiers	Specimen counts
Entandrophragma angolense	Fold 1: F31, M25766, M26523, M9034	16 (18)
	Fold 2: M2516, M25765, S44298	
	Fold 3: M37878, M41486, M9033	
	Fold 4: M17232, M36818, M9030	
	Fold 5: M9032, M9037, M40207	
Entandrophragma candollei	Fold 1: M4734, M9022, M9028, S21543	20 (20)
	Fold 2: M25762, M9021, M9026, S23275	
	Fold 3: M9025, S20558, S23578, T350	
	Fold 4: M16805, M3193, M9024, S48161	
	Fold 5: F36, M4725, M14732, M17230	
Entandrophragma cylindricum	Fold 1: B17123, F459, M14164, M25763, S48162	25 (20)
	Fold 2: B12209, M14146, M9014, M9015, T233	
	Fold 3: F44, M17226, M36764, M9012, M9013	
	Fold 4: B12219, M25764, M9016, S17097, S19750	
	Fold 5: F6, M9009, M9017, M9019, M9020	
Entandrophragma utile	Fold 1: B12207, M2506, M9007, S17114	20 (18)
	Fold 2: B18259, F3, M9003, M9008	
	Fold 3: B17124, M2483, M9004, S48164	
	Fold 4: M40208, M9005, S11130, S17098	
	Fold 5: B17520, T134, M17231, S46761	
Khaya anthotheca	Fold 1: M36767, S21549, S23268	14 (20)
	Fold 2: M2515, M9049, M9056	
	Fold 3: F100, M37605, M9048	
	Fold 4: M16996, M8699, M9055	
	Fold 5: M13411, S48166	
Khaya ivorensis	Fold 1: F240, M17960, M17963, S50022, S50023	25 (15)
	Fold 2: M8421, M8424, M9040, S50019, S50020	
	Fold 3: M8679, M9042, M9051, S16812, T11464	
	Fold 4: M17962, M37883, S16817, S33732, S48168	
	Fold 5: M8423, M9044, M17964, M17965, S50018	
Lovoa trichilioides	Fold 1: F10, M21538, M9088, S4119	19 (20)
	Fold 2: F39, M36802, M40184, S17103	
	Fold 3: B17473, M17198, M19344, T533	
	Fold 4: F135, M13582, S48169, S48515	
	Fold 5: B18269, F86, S27612	
Swietenia humilis	Fold 1: M33827, S5359, T29325	13 (12)
	Fold 2: M8678, S4765, S8902	
	Fold 3: S10364, S7483, S7484	
	Fold 4: M725, S5894	
	Fold 5: M11879, S3060	

Table 1 (continued)

Species	Accession identifiers	Specimen counts
Swietenia macrophylla	Fold 1: M16402, S16351, S350, S4428, S6631	25 (17)
	Fold 2: M19340, M4039, M8566, S16813, S17118	
	Fold 3: S152, S16814, S16815, S5966, S7800	
	Fold 4: S2056, S21015, S21092, S21093, T3792	
	Fold 5: S141, M16046, S7720, S17117, S21094	
Swietenia mahagoni	Fold 1: M19356, M20828, M2671, M7264	16 (15)
	Fold 2: M11039, M3905, M3939	
	Fold 3: M19339, M33825, M8676	
	Fold 4: M18263, M4780, M8677	
	Fold 5: M1203, M2676, M10139	

Entries in the specimen counts column have the format: number of specimens for the XyloTron model (number of specimens in Deklerck et al. 2019). The prefixes M, S, F, T, and B in the accession identifiers column refer to MADw, SJRw, FORIGw, Tw, and BCTw collections, respectively

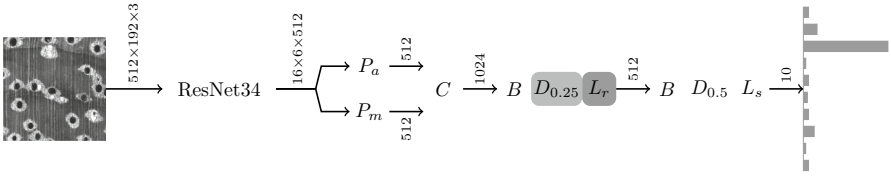

Fig. 1 Architecture of the CNN used. The input is a digital image, and the output is a vector of prediction probabilities of length 10. P_a: global average pooling layer, P_m: global max pooling layer, C: concatenation layer, B: batchnorm layer, D_p: dropout layer with probability p, L_r: fully connected layer with ReLU activation, L_s: fully connected layer with softmax activation

Model training

A two-stage transfer learning process was used for model training. In the first stage, the ResNet34 backbone was initialized with ImageNet pretrained weights (He et al. 2016) and the custom head was initialized using He normalization (He et al. 2015). During this stage, the custom head was trained for 6 epochs, while the ResNet backbone was used as a feature extractor with the weights frozen. In the second stage, the parameters of the entire network were trained for 8 epochs. The Adam optimizer (Kingma and Ba 2014) with simultaneous annealing of the learning rate (between $\alpha_{\max}$ and $\alpha_{\min}$) and momentum (between $\beta_{\max}$ and $\beta_{\min}$) (Smith 2018; Howard et al. 2018) was employed for both stages. Random 512×192 pixel patches (obtained by $4\times$ downsampling of 2048×768 pixel patches) were input to the network in mini-batches of size 16 with a data augmentation strategy that included horizontal and vertical reflections, random rotations in the range $[-5, 5]$ degrees and cutout (Devries and Taylor 2017). It should be reiterated that the training methodology and training

hyperparameters are exactly the same as in Ravindran et al. (2019) and that no data set specific hyperparameter tuning was performed. The hyperparameter values are summarized in Table 2. PyTorch (Paszke et al. 2019), and scientific Python packages (Jones et al. 2014) were used to train the model on a NVIDIA Titan X GPU.

Notation

Let $f \in \{1, \ldots F\}$ and $s \in \{1, \ldots S\}$ where F and S are the number of folds and seeds, respectively. If $C^{(s,f)}$ is the confusion matrix for fold f with model initialization seed s, the confusion matrix (over the five folds) for seed s, $C^{(s)}$, was computed as:

$$C^{(s)} = \sum_{f=1}^{F} C^{(s,f)}.$$

The corresponding prediction accuracy of the model is computed from the confusion matrix as:

$$A^{(s)} = \frac{\sum_i C_{ii}^{(s)}}{\sum_{i,j} C_{ij}^{(s)}}.$$

Some useful statistics are:

$$\begin{aligned} A &= \texttt{maximum}(\{A^{(s)} | s \in \{1, \ldots S\}\}), \\ A_\mu &= \mu(\{A^{(s)} | s \in \{1, \ldots S\}\}) \text{ (mean accuracy)}, \\ A_\sigma &= \sigma(\{A^{(s)} | s \in \{1, \ldots S\}\}), \text{ (standard deviation in accuracies)}. \end{aligned}$$

Experiments

Fivefold cross-validation ($F = 5$) was used for model evaluation with specimen-level splits, i.e., every specimen contributed images to exactly one fold (Table 1).

Table 2 Listing of training hyperparameters. The settings are the same as in Ravindran et al. (2019), and no data set specific hyperparameter tuning was performed

Hyperparameter	Value
Patch size	512×192 (pixels)
Minibatch size	16
Number of epochs (stage 1)	6
Number of epochs (stage 2)	8
$\alpha_{\max}$ (stage 1)	$2e^{-2}$
$\alpha_{\max}$ (stage 2)	$1e^{-5}$
$\alpha_{\min}$ (stages 1, 2)	$\alpha_{\max}/10$
$\beta_{\max}$	0.95
$\beta_{\min}$	0.85

In addition, the model parameters were initialized from five different seeds ($S = 5$), and for each of these initializations, the cross-validation procedure was repeated. During testing, the model prediction scores on the central 512×192 pixel patch (obtained by 4× downsampling of the central 2048×768 pixel patch) for every image in the test fold were obtained. The prediction for each image was the label with maximum prediction score on its central patch, and the specimen prediction was the majority prediction of its images.

Metrics from Deklerck et al.

Deklerck et al. (2019) report results that appear to correspond to the case $F = 5, S = 1$ and provide a confusion matrix corresponding to their best hyperparameters for their random forest model (figure 3 in Deklerck et al. 2019)—this confusion matrix was used to compute and report $A = A^{(s)}$. Since $S = 1$, it precluded the computation of mean accuracy (and the standard deviation) (Table 3).

Results and discussion

Results

At the species level, the accuracy of the XyloTron model (averaged over the 5 seeds, i.e., $A_\mu \pm A_\sigma$) was $81.9 \pm 0.8\%$. The accuracy of the model from the best seed was 82.4%. In order to take the most conservative approach possible, Fig. 2 presents the species-level confusion matrix from the worst performing seed, which shows that most errors are still within the correct genus. Genus-level predictions were derived from the species-level predictions, where out-of-species-but-within-genus predictions were considered correct whereas out-of-genus predictions were considered incorrect. The genus-level accuracy of the XyloTron model was $96.1 \pm 0.8\%$. The corresponding species- and genus-level accuracies calculated from figure 3 in Deklerck et al. (2019) were 74.9% and 91.4%, respectively. In Fig. 3, the genus-level confusion matrices for the XyloTron model and the DART model of Deklerck et al. (2019) are shown for side-by-side comparison.

Table 3 Prediction accuracies computed from the confusion matrices: XyloTron and DART from Deklerck et al. (2019)

	XyloTron (%)	DART Deklerck et al. (2019) (%)
Species-level accuracy	81.9 ± 0.8	74.9*
Genus-level accuracy	96.1 ± 0.8	91.4

*Additionally, Deklerck et al. (2019) report an accuracy of 82.2% for their best model

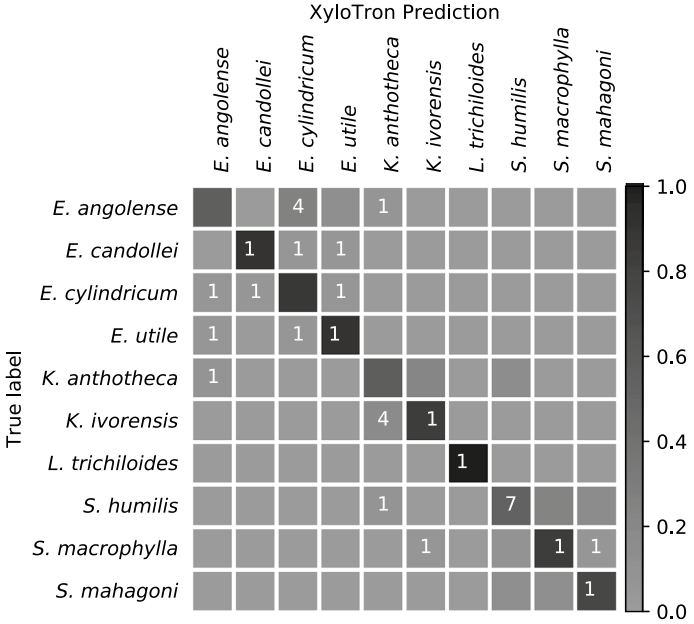

Fig. 2 Species-level confusion matrix for the worst performing seed. Cell colors are coded by accuracy proportions. Cells with nonzero specimen counts are annotated. The species-level accuracy computed from this confusion matrix is 80.3%

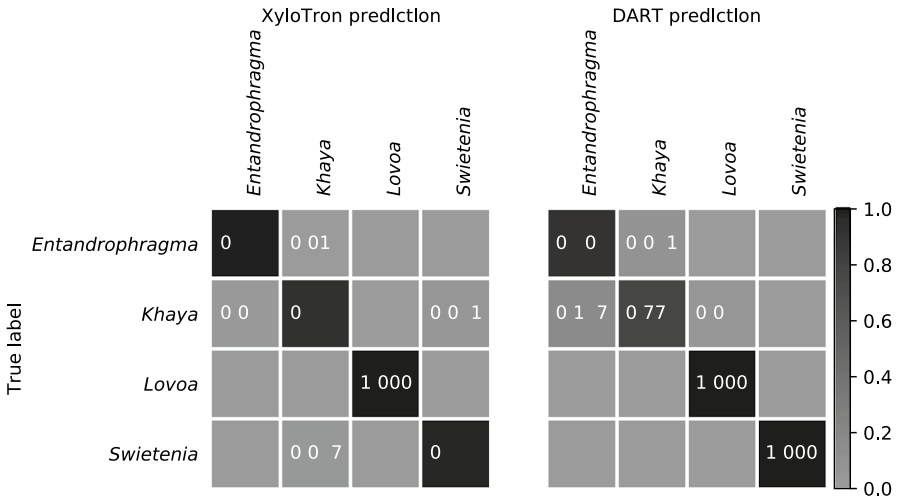

Fig. 3 Genus-level confusion matrices. Left: confusion matrix (worst performing seed) of the XyloTron model. Right: confusion matrix of Deklerck et al. (2019). Cells with nonzero proportions are annotated. Prediction accuracies are displayed as proportions because the number of specimens used for the two methods is not the same (Table 1)

Discussion

To the authors' best knowledge, this is the first work making side-by-side comparison of disparate—and putatively complementary—forensic wood identification techniques, computer vision and mass spectrometry. The XyloTron computer vision wood identification models performed at the same (species-level) or higher (genus-level) accuracy as DART mass spectrometry for the 10 Meliaceae woods studied. The species-level accuracy of the average of the XyloTron models over five folds and seeds (81.9%) is comparable with the best accuracy of 82.2% reported by Deklerck et al. (2019) and is higher than the species-level accuracy of 74.9% computed from their confusion matrix. The genus-level accuracy of the XyloTron model is 4.7 percentage points higher than the DART genus-level accuracy calculated from their confusion matrix. These are the first known results demonstrating comparable or better accuracy metrics for computer vision compared with DART data for wood discrimination.

It can be argued that the most relevant way to compare methods would be to test them on the same specimens, rather than merely the same species. Logistical challenges notwithstanding, there is merit to this argument. A given set of reference specimens could potentially exhibit low variability with one technique and high variability with another, but if any method purports to achieve species- or genus-specific identification, it is implicitly asserting a generalizable method that works across "all" instances of the taxon, not merely those in the reference data set. A method that correctly identifies only those specimens to which it had already been exposed would be of limited practical value.

Neither the results of the XyloTron model nor the results of Deklerck et al. (2019) give us any direct insight into how these models would perform in the real world. It is known that machine learning models perform better on their initial data set than on a comparable but new data set (Recht et al. 2019; Ravindran et al. 2019). Because of this, the next critical phase for model development studies is to demonstrate real-world applicability and efficacy by field-testing and ground-truthing. Correlating metrics from real-world tests back to in silico performance establishes the foundational scientific facts about the technology's performance. For some forensic applications, the operating context may always be one of species-level identification, but in other contexts, species-level identification may be desirable but not necessary. In that case, out-of-genus error may be much more practically significant than out-of-species-but-within-genus error. Which taxonomic scale to emphasize depends more on the context of eventual real-world deployment than on the scientific details of the models' accuracies.

When a program officer is selecting from several forensic wood identification technology options, they should consider more than just prediction accuracy. They must determine where, for what purposes, and at what scale a technology must serve, how the technology performs in the field, how scalable and cost-effective it is, the embodied costs of operator training, system calibration, and other logistical details (Dormontt et al. 2015; Schmitz et al. 2019). Access to these data is critical for making informed deployment decisions, and decision making depends necessarily on the ability to conduct side-by-side comparisons on the same sets of taxa. This

work here and that of Deklerck et al. (2019) provide no data addressing these issues, but as technologies evolve toward real-world deployment, these non-traditional, context-dependent performance metrics will become necessary data for evaluating disparate technologies.

Conclusion

To validly compare prediction accuracies between different technologies, the same taxa must be studied. For the case of the 10 Meliaceae woods evaluated here, the prediction accuracies of the XyloTron computer vision model equal or exceed those of the DART mass spectrometry method. In addition to prediction accuracies, prudent evaluation of wood forensic technologies should consider other factors such as needed granularity of discrimination, price point and scalability, necessity of specialized operator expertise, nature of forensic questions, field deployability, and real-world field performance.

Acknowledgements The authors would like to thank Richard Soares, Flavio Ruffinatto, Emmanuel Ebanyenle, Nic Bargren, Karl Kleinschmidt, and Adriana Costa for help with wood specimen preparation and imaging. The insightful comments of two anonymous reviewers helped clarify the narrative, and this is gratefully acknowledged.

Compliance with ethical standards

Conflict of interest The authors declare that they have no conflict of interest.

References

Akhmetzyanov L, Buras A, Sass-Klaassen U, Ouden J, Mohren G, Groenendijk P, García-González I (2019) Multi-variable approach pinpoints origin of oak wood with higher precision. J Biogeogr 46:1163–1177

Bergo M, Pastore T, Coradin V, Wiedenhoeft A, Braga J (2016) NIRS identification of *Swietenia macrophylla* is robust across specimens from 27 countries. IAWA J 37:420–430

Braun B (2013) Wildlife detector dogs—a guideline on the training of dogs to detect wildlife in trade. Technical report, WWF Germany

Cordeiro J, Martinez M, Li R, Cardoso A, Nunes L, Krug F, Paixão T, Nomura C, Gruber J (2012) Identification of four wood species by an electronic nose and by LIBS. Int J Electrochem 2012:5

da Silva NR, De Ridder M, Baetens JM, Van den Bulcke J, Rousseau M, Martinez Bruno O, Beeckman H, Van Acker J, De Baets B (2017) Automated classification of wood transverse cross-section micro-imagery from 77 commercial central-African timber species. Ann For Sci 74(2):30

Degen B, Ward S, Lemes M, Navarro C, Cavers S, Sebbenn A (2013) Verifying the geographic origin of mahogany (*Swietenia macrophylla* King) with DNA-fingerprints. Forensic Sci Int Genet 7(1):55–62

Deklerck V, Mortier T, Goeders N, Cody R, Waegeman W, Espinoza E, Van Acker J, Van den Bulcke J, Beeckman H (2019) A protocol for automated timber species identification using metabolome profiling. Wood Sci Technol 53(4):953–965

Devries T, Taylor GW (2017) Improved regularization of convolutional neural networks with cutout. CoRR 1708.04552

Dormontt EE, Boner M, Braun B, Breulmann G, Degen B, Espinoza E, Gardner S, Guillery P, Hermanson JC, Koch G, Lee SL, Kanashiro M, Rimbawanto A, Thomas D, Wiedenhoeft AC, Yin Y,

Zahnen J, Lowe AJ (2015) Forensic timber identification: it's time to integrate disciplines to combat illegal logging. Biol Conserv 191:790–798
Filho PL, Oliveira LS, Nisgoski S, Britto AS Jr (2014) Forest species recognition using macroscopic images. Mach Vis Appl 25(4):1019–1031
Finch K, Espinoza E, Jones F, Cronn R (2017) Source identification of western Oregon Douglas-fir wood cores using mass spectrometry and random forest classification. Appl Plant Sci 5:1600158
Gasson P (2011) How precise can wood identification be? Wood anatomy's role in support of the legal timber trade, especially CITES. IAWA J 32:137–154
Graham S (1997) Anatomy of the Lindbergh kidnapping. J Forensic Sci 42:368–377
Guo J, Xiao L, Han L, Wu H, Yang T, Wu S, Yin Y, Donaldson LA (2019) Deterioration of the cell wall in waterlogged wooden archeological artifacts, 2400 years old. IAWA J 40(4):820–844
He K, Zhang X, Ren S, Sun J (2015) Delving deep into rectifiers: surpassing human-level performance on ImageNet classification. In: Proceedings of the IEEE international conference on computer vision, pp 1026–1034, 1502.01852
He K, Zhang X, Ren S, Sun J (2016) Deep residual learning for image recognition. In: 2016 IEEE conference on computer vision and pattern recognition, pp 770–778
He T, Marco J, Soares R, Yin Y, Wiedenhoeft AC (2019) Machine learning models with quantitative wood anatomy data can discriminate between *Swietenia macrophylla* and *Swietenia mahagoni*. Forests 11(1):36
Hermanson JC, Dostal D, Destree JC, Wiedenhoeft AC (2019) The XyloScope—a field deployable macroscopic digital imaging device for wood. Research note FPL-RN-0367, U.S. Department of Agriculture, Forest Service, Forest Products Laboratory, p 18
Hinton GE, Srivastava N, Krizhevsky A, Sutskever I, Salakhutdinov R (2012) Improving neural networks by preventing co-adaptation of feature detectors. CoRR abs/1207.0580
Howard J et al (2018) fastai. https://github.com/fastai/fastai
Ioffe S, Szegedy C (2015) Batch normalization: accelerating deep network training by reducing internal covariate shift. CoRR abs/1502.03167
Jiao L, Yu M, Wiedenhoeft AC, He T, Li J, Liu B, Jiang X, Yin Y (2018) DNA barcode authentication and library development for the wood of six commercial Pterocarpus species: the critical role of xylarium specimens. Sci Rep 8:1945
Jiao L, Lu Y, He T, Li J, Yin Y (2019) A strategy for developing high-resolution DNA barcodes for species discrimination of wood specimens using the complete chloroplast genome of three Pterocarpus species. Planta 250(1):95–104
Jones E, Oliphant T, Peterson P (2014) SciPy: open source scientific tools for Python. wwwscipyorg
Kagawa A, Leavitt S (2010) Stable carbon isotopes of tree rings as a tool to pinpoint the geographic origin of timber. J Wood Sci 56(3):175–183
Khalid M, Lew E, Lee Y, Yusof R, Nadaraj M (2008) Design of an intelligent wood species recognition system. Int J Simul Syst Sci Technol 9:9–19
Kingma DP, Ba J (2014) Adam: A method for stochastic optimization. CoRR 1412.6980
Kite GC, Green PW, Veitch NC, Groves MC, Gasson PE, Simmonds MS (2010) Dalnigrin, a neoflavonoid marker for the identification of Brazilian rosewood (*Dalbergia nigra*) in CITES enforcement. Phytochemistry 71(10):1122–1131
Kress WJ (2017) Plant DNA barcodes: applications today and in the future. J Syst Evol 55(4):291–307
LeCun Y, Boser B, Denker JS, Henderson D, Howard RE, Hubbard W, Jackel LD (1989) Backpropagation applied to handwritten zip code recognition. Neural Comput 1(4):541–551
Lowe AJ, Dormontt EE, Bowie MJ, Degen B, Gardner S, Thomas D, Clarke C, Rimbawanto A, Wiedenhoeft A, Yin Y, Sasaki N (2016) Opportunities for improved transparency in the timber trade through scientific verification. Bioscience 66(11):990–998
Ma T, Inagaki T, Ban M, Tsuchikawa S (2018) Rapid identification of wood species by near-infrared spatially resolved spectroscopy (NIR-SRS) based on hyperspectral imaging (HSI). Holzforschung 73:323–330
Meier-Augenstein W (2019) From stable isotope ecology to forensic isotope ecology—isotopes' tales. Forensic Sci Int 300:89–98
Nair V, Hinton GE (2010) Rectified linear units improve restricted Boltzmann machines. In: Proceedings of the 27th international conference on machine learning, pp 807–814
Ostapkowicz J, Brock F, Wiedenhoeft AC, Snoeck C, Pouncett J, Baksh-Comeau Y, Schulting R, Claeys P, Mattielli N, Richards M, Boomert" A (2017) Black pitch, carved histories: radiocarbon dating,

wood species identification and strontium isotope analysis of prehistoric wood carvings from Trinidad's Pitch Lake. J Archaeol Sci Rep 16:341–358

Paszke A, Gross S, Massa F, Lerer A, Bradbury J, Chanan G, Killeen T, Lin Z, Gimelshein N, Antiga L, Desmaison A, Kopf A, Yang E, DeVito Z, Raison M, Tejani A, Chilamkurthy S, Steiner B, Fang L, Bai J, Chintala S (2019) Pytorch: an imperative style, high-performance deep learning library. Adv Neural Inf Process Syst 32:8024–8035

Pavlovich MJ, Musselman B, Hall AB (2018) Direct analysis in real time-mass spectrometry (DART-MS) in forensic and security applications. Mass Spectrom Rev 37(2):171–187

Ravindran P, Costa A, Soares R, Wiedenhoeft AC (2018) Classification of CITES-listed and other neotropical Meliaceae wood images using convolutional neural networks. Plant Methods 14(1):25

Ravindran P, Ebanyenle E, Ebeheakey AA, Abban KB, Lambog O, Soares R, Costa A, Wiedenhoeft AC (2019) Image based identification of Ghanaian timbers using the XyloTron: opportunities, risks and challenges. In: NeurIPS workshop on machine learning for the developing world (ML4D): challenges and risks. arXiv:1912.00296

Recht B, Roelofs R, Schmidt L, Shankar V (2019) Do imagenet classifiers generalize to imagenet? CoRR abs/1902.10811. https://arxiv.org/abs/1902.10811v2. Retrieved 19 March 2020

Ruffinatto F, Macchioni N, Boetto G, Baas P, Zanuttini R (2010) Reflected light microscopy as a non-invasive identification tool for wooden artefacts. IAWA J 31(3):317–331

Russakovsky O, Deng J, Su H, Krause J, Satheesh S, Ma S, Huang Z, Karpathy A, Khosla A, Bernstein M, Berg AC, Fei-Fei L (2015) ImageNet large scale visual recognition challenge. Int J Comput Vis 115(3):211–252

Schmitz N, Beeckman H, Cabezas JA, Cervera M, Espinoza E, Fernandez-Golfin J, Gasson P, Hermanson J, Arteaga M, Koch G, Lens F, Martínez-Jarquín S, Paredes K, Pastore T, Ramananantoandro T, Schraml R, Schroeder H, Sebbenn A, Tysklind N, Wiedenhoeft A (2019) The timber tracking tool infogram. overview of wood identification methods' capacity. Report global timber tracking network, GTTN Secretariat, European Forest Institute and Thünen Institute. https://doi.org/10.13140/RG.2.2.27920.25603

Smith LN (2018) A disciplined approach to neural network hyper-parameters: part 1—learning rate, batch size, momentum, and weight decay. CoRR abs/1803.09820. http://arxiv.org/abs/1803.09820. 1803.09820

Snel F, Braga J, da Silva D, Wiedenhoeft A, Costa A, Soares R, Coradin V, Pastore T (2018) Potential field-deployable NIRS identification of seven Dalbergia species listed by CITES. Wood Sci Technol 52:1411–1427

Vlam M, de Groot GA, Boom A, Copini P, Laros I, Veldhuijzen K, Zakamdi D, Zuidema PA (2018) Developing forensic tools for an African timber: regional origin is revealed by genetic characteristics, but not by isotopic signature. Biol Conserv 220:262–271

Wiedenhoeft AC, Kretschmann DE (2014) Species identification and design value estimation of wooden members in covered bridges. Technical report, FPL-GTR-228, U.S. Department of Agriculture, Forest Service, Forest Products Laboratory

Wiedenhoeft AC, Simeone J, Smith A, Parker-Forney M, Soares R, Fishman A (2019) Fraud and misrepresentation in retail forest products exceeds U.S. forensic wood science capacity. PLOS ONE 14(7):1–13

Zhang M, Zhao G, Guo J, Liu B, Jiang X, Yin Y (2019) A GC-MS protocol for separating endangered and non-endangered Pterocarpus wood species. Molecules 24(4):799